Annealing effect on ZnO-NPs buffer layer assembled organic solar cells synthesized with CuO nanoparticles

Aruna P. Wanninayake, Benjamin C. Church, Nidal Abu-Zahra*

Materials Science and Engineering Department, University of Wisconsin-Milwaukee, 3200 North Cramer Street, Milwaukee, WI 53201, USA

*Corresponding author, E-mail: nidal@uwm.edu

Abstract

Organic solar cells were fabricated with varying amounts of ZnO-NPs in a buffer layer located over an active layer of P3HT/PCBM incorporating a fixed amount of CuO nanoparticles. The buffer layer serves as an electron transporting layer in the device. Thermal annealing treatment was applied to all the devices at different temperatures (150ºC, 200ºC and 250ºC) to optimize the nanoscale morphology. The samples which were annealed at 200ºC exhibited the best power conversion performance. The enhanced morphological and optoelectronic properties attained by applying thermal annealing, increased the power conversion efficiency by 14.6% compared to a reference cell. The ZnO-NPs buffer layer improved the exciton dissociation rate, electron mobility, optical absorption and charge collection at the anode, resulting in higher short circuit currents and external quantum efficiencies. The short circuit current (J_{sc}) of the optimum device was measured at 8.949mA/cm^2 compared to 7.62 mA/cm^2 in the reference cell before annealing. Meanwhile, the external quantum efficiency (EQE) increased from 61.8% to 62.9%, after thermal annealing. Copyright © 2016 VBRI Press.

Keywords: ZnO nanoparticles, CuO nanoparticles, EQE, thermal annealing, PSCs, OSCs.

Introduction

Organic solar cells (OSCs), which are based on interpenetrating network of conjugated polymer donor and fullerene derivative acceptor materials, have attracted much attention in recent years due to their advantages of easy fabrication, simple device structure, low cost, light weight, and capability to be fabricated into flexible devices [1-4]. The power conversion efficiency (PCE) of OSCs has been investigated through multidisciplinary attempts including designing new device structures, applying low band gap materials, and carefully controlling the morphology of the donor-acceptor molecular structure [5, 6]. Among these efforts, optimization of the nano-morphology of the low-bandgap conjugated polymers has proved to be crucial for improving the power conversion efficiency of these devices.

The nano-morphology of the active polymer determines the donor-acceptor (D/A) molecular arrangement and phase separation within thin films. Hence, morphologically optimized thin films enhance the photon absorption, carrier mobility and exciton dissociation mechanisms. Many researchers worked on enhancing the PCE of polymer based solar cells by various approaches. These include the design of novel device structures, synthesizing materials with short energy gaps, refining the morphology of active layers, upgrading photon generation ability, and increasing electron-hole mobility by adjusting D-A contact surfaces [7]. To enhance the molecular ordering and surface morphology in spun-casted polymer films, several strategies; such as thermal and solvent annealing [8] and doping additives [9] have been used successfully. This in turn will increase the light harvesting capacity of P3HT: PCBM films and improve their power conversion efficiencies. Motaung *et al.* [10] obtained 1.03% maximum PCE for ZnO incorporated P3HT: PCBM devices which were heat treated up to 140°C. Kang *et al.* [11] reported 3.86% PCE, 0.68V open-circuit voltage (V_{oc}) and 64% fill factor (FF) through post-annealing at 170°C. CuO NPs were successfully incorporated into the P3HT/ PC70BM active layer by our research group. The PCE of cells with 0.6 mg CuO NPs increased by 40.9% due to enhanced carrier generation ability of the P3HT: PCBM film [12, 13].

Optimization of the nano-morphology of the inorganic thin films remarkably improves their optical and electronic properties. Thermal annealing techniques are widely used in organic as well as inorganic thin film solar cells to enhance their electrical and optical properties by enhancing crystallinity, reducing defects, and roughening the crystalline phases in the thin films [14-16]. Inorganic materials such as TiO$_2$ [17], CdSe, CsCO$_3$ [18], and ZnO [19] are considered among the most effective electron acceptor materials. Solution-processed ZnO nanostructure thin films have demonstrated efficient carrier

extracting/transporting ability and promising hole blocking capacity [20]. Liu *et al.* [21] have reported that the annealing process improved the PCE to 3.43% of ZnO buffer layer embedded OSCs.

This study demonstrates the enhancement of power conversion efficiency of CuO NPs incorporated P3HT/PC70BM PSCs containing a ZnO-NPs buffer layer with thermal annealing treatment. The combined effect of CuO and ZnO-NPs was studied by UV–visible analysis, current voltage (J–V) characteristics, atomic force microscopy, and EQE measurements. In addition the electrical performance of the hybrid solar devices is presented in this work.

Experimental

Materials

Glass substrates measuring 24 x 80 x 1.2 mm (12 Ω/cm^2) with an ITO conductive layer of 25-100 nm were purchased from nanocs.com. PEDOT/PSS mixed in distilled water was obtained from Sigma Aldrich and it was mixed with an equal amount of distilled water. Active layer materials, P3HT and PC70BM were purchased from Rieke Metals and SES Research; respectively. Nanoparticles of ZnO (18 nm diameter) and CuO (100 to 150nm diameter) were purchased from nanocs.com. Aluminium coils with a diameter of 0.15 mm were purchased from Ted-Pella, Inc. (tedpella.com). All processing and characterization work of the PSC devices were conducted under same experimental conditions.

Solar cells fabrication

The conductive glass substrates were ultrasonically cleaned with ammonium hydroxide, hydrogen peroxide, distilled water, methyl alcohol, and isopropyl alcohol successively. The fabrication of polymer based solar cells containing Zinc oxide and Copper oxide NPs was done in a N$_2$ filled glove box. The P3HT-PC70BM blend was obtained by diluting same amounts of regioregular P3HT and PC70BM (10 mg each) with 2ml of chlorobenzene (C$_6$H$_5$Cl) and mixing for 14 hours at 60ºC. CuO NPs were dispersed in 2ml of C$_6$H$_5$Cl and were added to the mixture, so that the weight ratios of P3HT/PCBM/CuO-NPs in the final blend was 10:10:0.6 mg. Different amounts of ZnO nanoparticles were dispersed in pure ethanol to make four solutions with concentrations of 10, 20, 30, and 40 mg ml^{-1} of NPs.

The structure of the fabricated solar cell devices is schematically presented in **Fig. 1**. The solar cell devices were spun coated in a glove box with N$_2$ atmosphere. A 40 nm-thick PEDOT/PSS layer, which serves as a thin hole-transport layer, was spun coated at a rotational velocity of 4000 rpm, followed by heating at 120°C for 20 minutes in air. When the temperature of the samples reached the ambient temperature, the blends with P3HT:PC70BM: CuO NPs and ZnO solution were spun coated for two minutes at 1000 rpm and 2000 rpm; respectively. In this study, five different devices (reference cell, 10, 20, 30 and 40 mg ml^{-1} ZnO NPs in the buffer layer) were fabricated. The active layers measured 120 nm in average thickness and 0.12 cm^2 in surface area. Annealing was performed on all devices, after Al

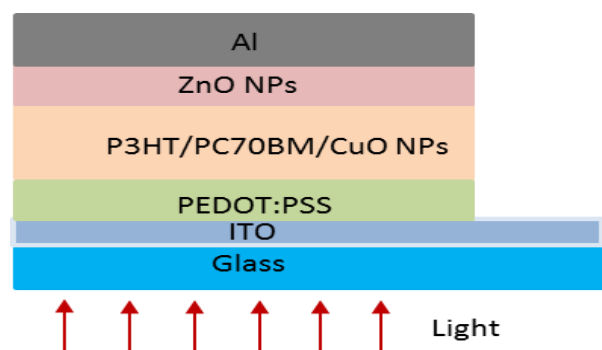electrode deposition, inside an inert oven at 150ºC, 200°C and 250°C for 30 minutes.

Fig. 1. Graphical representation of the hybrid device architecture.

Solar cells characterization

The current density–voltage (J-V) characterization was carried out for all PSCs using a UV solar simulator with an AM 1.5G filter and a lamp intensity of 100 mW/cm^2. A source meter (Keithley 2400) was used to obtain the J-V measurements. Device parameters such as short circuit current (J_{sc}), open circuit voltage (V_{oc}), fill factor (FF) and power conversion efficiency (PCE) were recorded under ambient conditions. A quantum efficiency measurement kit (Newport-425) embedded in the solar cell simulator was used to obtain EQE values. A PerkinElmer LAMBDA 650 spectrophotometer was used to obtain the optical properties of cells containing varying amounts of ZnO NPs. Crystallinity studies of the thin layers were performed by XRD with a Cu/K source at a rate of 0.2° per minute. Recorded range of the X-ray spectra were from 4° - 7°. Agilent 5420 atomic force microscope (AFM) was used to analyze the surface morphology of the devices. Pico Image Basics and Gwyddion software were used to determine the root mean square surface roughness (σ_{rms}).

Results and discussion

The performance characteristics of the devices which contain 0.6mg of CuO NPs and varying amounts of ZnO NPs in the buffer layer were measured after annealing at 200℃ for 30 minutes. The photovoltaic parameters such as short-circuit current density (J_{sc}), open-circuit voltage (V_{oc}), fill factor ($FF = \frac{J_m V_m}{J_{sc} V_{oc}}$), and power conversion efficiency; which is defined as the ratio of the products of V_{oc}, J_{sc} and FF to the total incident power density ($PCE = \eta = \frac{J_{sc} V_{oc} FF}{P_{in}}$) [22, 23], are shown in **Table 1**.

Table 1. Performance parameters of PEDOT: PSS/P3HT/PCBM/CuO-NP/ZnO NPs hybrid solar cells before and after heat treatment at 200°C for 30 minutes.

ZnO NPs (mg)	J_{sc} (mA/cm^2) Before Annealing	After Annealing	V_{oc} (V) Before Annealing	After Annealing	FF (%) Before Annealing	After Annealing	PCE (%) Before Annealing	After Annealing
0	6.480	7.777	0.677	0.679	68.11	69.53	2.988	3.672
10	7.063	8.890	0.688	0.680	71.44	71.62	3.472	4.330
20	7.620	8.949	0.696	0.678	74.47	74.77	3.950	4.530
30	7.437	8.810	0.702	0.681	72.46	74.40	3.784	4.464
40	7.379	8.107	0.714	0.683	69.79	69.88	3.677	3.875

The J-V characteristic parameters of the reference devices (0mg ZnO-NPs) after annealing revealed J_{sc} of 7.777 mA/cm². It increased to 8.949 mA/cm² after assembling a buffer layer containing 20 mg of ZnO NPs, an enhancement of 15%. This enhanced short circuit current density proportionally improved the PCE from 3.672% to 4.530%. Following a similar trend, the fill factor increased from 69.53 to 74.77% after annealing treatments. The devices before annealing exhibited PCE of 2.988% in the reference device and it improved to 3.950% with ZnO nanostructured buffer layer. The thermal annealing treatment contributed for about 23% increase in PCE as a result of notably improved J_{sc} and FF. However, the open-circuit voltage (V_{oc}) did not change significantly before and after annealing treatments. Based on power conversion efficiency equation (PCE = $V_{oc}*J_{sc}*FF$/total incident power density) V_{oc}, J_{sc}, and FF are significant factors in determining the overall PCE. Higher V_{oc}, J_{sc}, and FF result in higher PCE. The current density-voltage $(J-V)$ characteristics of the solar cells before and after annealing are shown in **Fig. 2**.
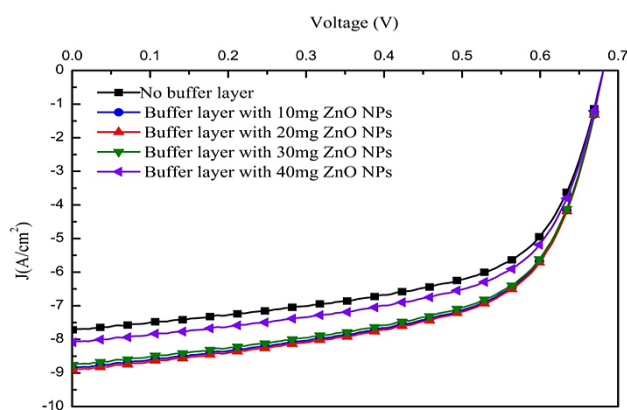

Fig. 2. *J-V* characteristics of hybrid polymer solar cells with ZnO buffer layer after annealing.

The solar cell devices assembled with a ZnO buffer layer (20mg of NPs) and 0.6mg of CuO NPs were annealed at three different temperatures: 150ºC, 200ºC and 250ºC for 30 minutes. The performance characteristics of these devices are summarized in **Table 2**. At all annealing temperatures, the devices show a significant improvement of PCEs compared to the devices without annealing treatment. The devices annealed at 200ºC for 30 minutes exhibit the optimum performance. However, the lowest short circuit current density (J_{sc}) of 8.186 mA/cm², open circuit voltage (V_{oc}) of 0.674 V, filling factor (FF) of 69.05%, and PCE of 3.81% were obtained from the devices annealed at 250ºC. The devices annealed at 150ºC, exhibited J_{sc}, V_{oc}, FF and PCE of 8.870 mA/cm², 0.675 V, 71.40% and 4.275% respectively.

Table 2. Performance characteristics of polymer solar cells with different annealing temperatures.

Temperature (ºC)	J_{sc} (A/cm²)	V_{oc} (V)	FF (%)	PCE (%)
150	8.870	0.675	71.40	4.275
200	8.949	0.678	74.77	4.530
250	8.186	0.674	69.05	3.810

The J_{sc} improvement is closely related to the EQE trend. The EQE or the incident photon to current conversion efficiency (IPCE) measurements describe the ratio between the incident photons on the solar cell, from the input source, and the generated free charge carriers by the solar cell. The enhanced efficiency factors of light absorption, exciton dissociation, carrier collection at the electrodes and charge carrier mobility strongly affect the EQE measurements. The corresponding EQE measurements (peak values) are shown in **Fig. 3**. When the particle densities in the ZnO buffer layer were increased, the relevant EQEs proportionally increased in the wavelength range from 310nm to 650nm. Before annealing, the devices had highest EQEs of 54.6%, 56.8%, 61.8%, 60% and 57.7% respectively. However, after annealing the peak values of the EQE for samples with 0 mg-ZnO, 10 mg-ZnO, 20 mg-ZnO, 30 mg-ZnO, and 40 mg-ZnO were 55.5%, 57.8%, 62.9%, 61.4% and 56.7% respectively.
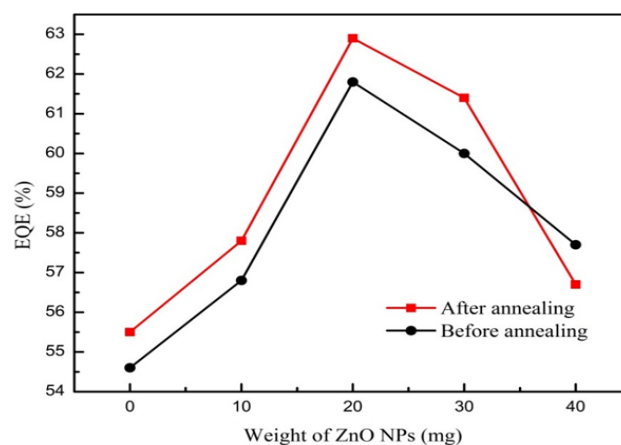

Fig. 3. Effect of thermal annealing on the EQE values of PSCs with ZnO buffer layer.

The P3HT/PCBM/CuO NPs structure provides two main electron-transporting paths: a conventional path through the PCBM molecules and hopping sites created by CuO NPs. The CuO NPs produce dense PCBM clusters with hopping sites creating an efficient electron flow towards the ZnO electron transport layer. The enhancement of EQE measurements is generally attributed to improved PCBM molecules. The ZnO electron transport buffer layer provides extremely high electron transporting facility to the Al electrodes uplifting the EQE profile. Therefore, the separated free electrons from excitons created in P3HT and CuO NPs phases can be transported through interconnected PCBM domains and CuO NPs hopping centers towards the ZnO buffer layer. Compared to the electron mobility in TiO$_x$ thin films (1.7 x 10⁻⁴ cm² V⁻¹ s⁻¹) [24], the ZnO NPs layers have higher electron mobility (6.6x 10⁻² cm² V⁻¹ s⁻¹) [25]. Hence, ZnO structure gives high momentum to the electrons towards the cathode. As a result, the electron mobility is remarkably enhanced resulting in a higher EQE. However, at higher concentrations of ZnO NPs, the EQE starts to decrease. This decline could be due to the excess amount of ZnO NPs (more than 20mg of ZnO NPs) diffusing into the active layer and changing the P3HT/PCBM nanoscale morphology which leads to

minimization of the exciton dissociation and enhance the nanoparticles agglomeration at the active layer.

To further study the effect of heat treatment on the optical properties of ZnO buffer layer assembled P3HT/PC70BM/0.6mg-CuO NPs PSCs the UV visible absorption spectra were obtained as shown in **Fig. 4**. After thermal annealing, the absorption intensities of all devices were enhanced. The optical absorption peak intensity of the P3HT/PC70BM/CuO NPs thin layer is 0.64 and after ZnO NPs buffer layer assembling the absorption intensity was improved to 0.76. However, the annealing treatment of the ZnO NPs buffer layer assembled P3HT/PC70BM/ CuO NPs devices increased the absorption intensity to 0.81. Consequently, the CuO NPs, ZnO NPs as well as thermal annealing led to higher optical absorption in the solar cells over the entire wavelength range. The increased absorption intensities are attributed to the enhanced crystallinity of P3HT by thermal annealing combined with improved optical absorption caused by CuO/ZnO NPs incorporated in the solar cell devices. Improved optical absorption yields higher charge carrier generation rate, better carrier mobility, and higher carrier injection to the electrodes resulting in better power conversion efficiency of the solar devices **[26, 27].**
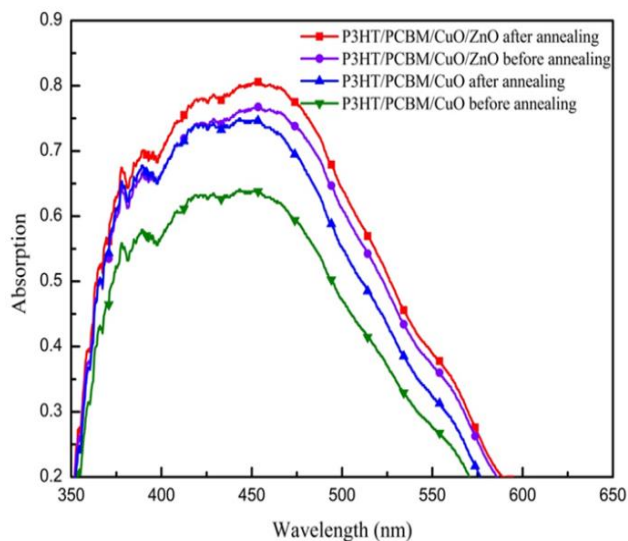

Fig. 4. Optical absorption spectra of PSCs with CuO and ZnO NPs before and after annealing.

The XRD spectra of the P3HT/PC70BM/0.6mg-CuO NPs samples were obtained before and after thermal annealing. The XRD spectra, shown in **Fig. 5**, illustrate improved peak intensities over the 2θ range from 4.5° to 6°. The increased diffraction peaks for P3HT: PC70BM: CuO NPs thin films are contributed to the improved self-organization of P3HT molecules leading to higher crystallinity. It is well known that P3HT and PC70BM are crystalline and amorphous materials respectively. Therefore, P3HT/PC70BM and CuO NPs blend is a partially crystalline structure. The thermal annealing of 0.6mg-CuO NPs facilitate P3HT chains to escape from the amorphous phase and rearrange as separate molecules within the polymer blend leading to P3HT/ PC70BM phase separation **[28, 29].**
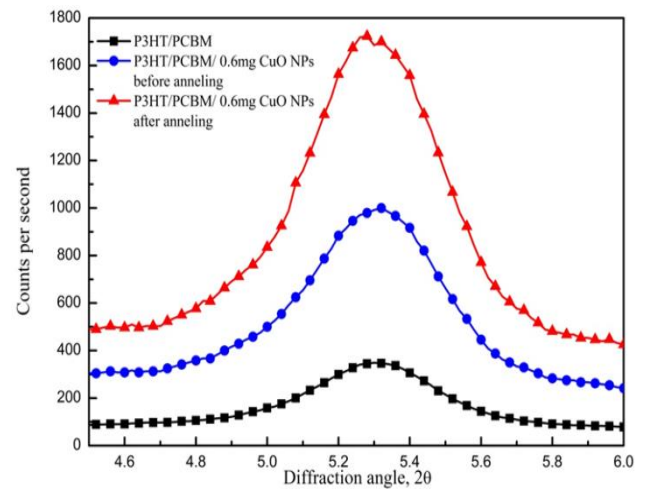

Fig. 5. XRD spectra for 0.6 mg of CuO NPs incorporated P3HT/PCBM thin films.

Surface morphological studies of the active layers were carried out using AFM. AFM images presented in **Fig. 6** show that thermal annealing increases the surface roughness of the nanostructured ZnO films which is assembled on the P3HT/PC70BM/CuO NPs thin film.
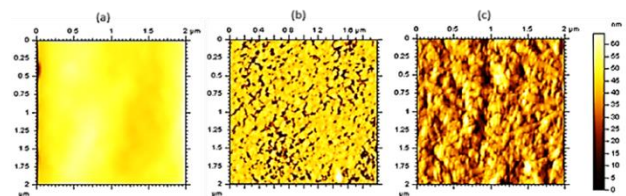

Fig. 6. AFM images of active layer: (a) P3HT/PC70BM/0.6mg CuO NPs (b) P3HT/PCBM/CuO-0.6mg NPs with 20mg of ZnO NPs buffer layer (c) P3HT/PCBM/CuO-0.6mg NPs with 20mg of ZnO NPs buffer layer after annealing.

The measured root-mean-square roughness (σ_{rms}) value of the P3HT/PC70BM/CuO layer was 0.33nm and after depositing the ZnO NPs layer on the active layer, the σ_{rms} value increased to 0.91nm. However, after annealing the optimum sample (P3HT/PCBM/0.6mg-CuO NPs with 20mg of ZnO NPs) exhibited a maximum surface roughness of 1.12nm. The rougher surfaces increase the interfacial contact area with the Al layer leading to higher charge collection ability at the Al cathode. Also, enhanced roughness can result in greater light absorption due to the diffuse reflection between the active layer and the cathode. Therefore, annealing of nanostructured ZnO thin films at 200ºC for 30 minutes optimizes the surface condition of the thin layers.
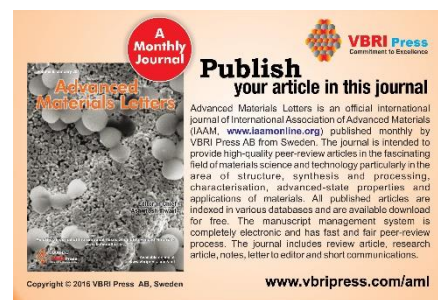
Conclusion

A nanostructured ZnO buffer layer was assembled as an electron transport layer on top of a P3HT/PC70BM/0.6mg-CuO NPs active layer. The devices which were thermally annealed at 200ºC for 30 minutes exhibited the optimum performance. The PCE for the cells containing 20mg of ZnO-NPs increased from 3.95% to 4.53% after heat treatment at 200℃ for 30 minutes. The improved performance is attributed to enhanced EQE, electron mobility, surface roughness and

optical absorption due to the presence of CuO and ZnO NPs in the devices. In addition, the optical absorption spectrum exhibited significant improvement after thermal annealing treatment due to the elevated exciton generation rate. AFM analysis shows an increase in surface roughness of the ZnO nanoparticles incorporated electron transport buffer layer after thermal annealing. The enhanced roughness results in greater light absorption due to the diffuse reflection between the active layer and the cathode which results in a larger interfacial contact area between ZnO and the Al cathode leading to higher charge collection ability at the Al cathode.

References

1. Dang, M.T.; Hirsch, L.; and Wantz, G. *Adv. Mater*, **2011**, *23*, 3597.
   DOI: 10.1002/adma.201100792
2. Wang, P.H.; Lee, H.F.; Huang, Y.C.; Jung, Y.J.; Gong, F.L.; and Huang, W.Y. *Electron. Mater. Lett.* **2014**, *10*, 767.
3. Martin, W.; Cordula, D. W.; Jonas, H.; Erik, A.; Gunther, G.; Mika, L.; Gisela, S.; Elena, M.; Amaresh, M.; Peter, B. *Chem. Commun.,* **2013**, *49*, 10865
4. Amaresh, M.; Markus, K. R. F.; Peter, B. Metal-Free Organic Dyes for Dye-Sensitized Solar Cells: From Structure: Property Relationships to Design Rules, *Angewandte Chemie,* **2009**, *48*, 2474.
   DOI: 10.1002/anie.200804709
5. Li, G.; Shrotriya, V.; Huang, J.; Yao, Y. *Nature Materials*, **2005**, *4*, 864.
   DOI: 10.1038/nmat1500
6. Li, G.; Zhu, R.; Yang, Y. *Nature Photonics*, **2012**, *6*, 153.
   DOI: 10.1038/nphoton.2012.11
7. Wicklein, A.; Ghosh, S.; Sommer, M.; Wurthner, F.; Thelakkat, M. *ACS Nano*, **2009**, *3*, 1107.
   DOI: 10.1021/nn9001165
8. Lee, W.H.; Chuang, S.Y.; Chen, H.L.; Su, W.F.; Lin, C.H. *Thin Solid Films*, **2010**, *518*, 7450.
   DOI: 10.1016/j.tsf.2010.05.021
9. Salim, T.; Wong, L.H.; Brauer, B.; Kukreja, R.; Foo, Y.L.; Bao, Z.; Lam, Y.M. *J. Mater. Chem.*, **2011**, *21*, 242.
   DOI: 10.1039/C0JM01976C
10. Motaung, D. E.; Malgas, G. F.; Ray, S.S; Arendse, C.J. *Thin Solid Films,* **2013**, *537*, 90.
    DOI: 10.1016/j.tsf.2013.04.037
11. Kang, R.; Oh, S.; Na, S.; Kim, T.S.; Kim, D.Y. *Sol. Energ. Mat. Sol. Cells,* **2014**, *120*, 131.
    DOI: 10.1016/j.solmat.2013.08.026
12. Wanninayake, A.P.; Gunashekar, S.; Li, S.; Church, B.C.; Abu-Zahra, N. *J. Sol. Energy Eng.* **2015**, *137*, 031016.
    DOI: 10.1115/1.4029542
13. Wanninayake, A.; Gunashekar, S.; Li, S.; Church, B.C.; Abu-Zahra, N. *Semicond. Sci. Technol.*, **2015**, *30*, 064004.
    DOI: 10.1088/0268-1242/30/6/064004
14. Niki, S.; Contreras, M.; Repins, I.; Powalla, M.; Kushiya, K.; Ishizuka, S.; Matsubara, K. *Prog. Photovolt. Res. Appl.*, **2010**, *18*, 453.
    DOI: 10.1002/pip.969
15. Venkatachalam, M.; Kannan, M.D., Jayakumar, S., Balasundaraprabhu, R.; Muthukumarasamy, N. *Thin Solid Films*, **2008,** 516, 6848.
    DOI: 10.1016/j.tsf.2007.12.127
16. Yang, W.; Duan, H.S.; Cha, K.C.; Hsu, C. J.; Hsu, W. C.; Zhou, H.; Bob, B.; Yang Y. *J Am Chem Soc.* **2013**, *135*, 6915.
    DOI: 10.1021/ja312678c
17. Mor, G.K.; Shankar, K.; Paulose, M.; Vargheseand, O.K.; Grimes, C.A., *Applied Physics Letters*, **2007,** *91*, 152111.
    DOI: 10.1063/1.2799257
18. Liao, H.H.; Chen, L.M.; Xu, Z.; Li, G.; Yang, Y. *Applied Physics Letters*, **2008**, *92*, 173303.
19. White, M.S.; Olson, D.C; Shaheen, S.E.; Kopidakis, N.; Ginley, D.S. *Applied Physics Letters*, **2006**, *89*, 143517.
20. Vayssieres L. *Advanced Materials*, **2003**, *15*, 464.
    DOI: 10.1002/adma.200390108
21. Liu, C.; Zheng, L.; Gao, Z.; Gan, Y.; Zhang, J.; Li, C. *Optics and Photonics Journal*, **2013**, *3*, 222.
22. Chen, X.; Zuo, L.; Fu, W.; Yan, Q.; Fan, C.; Chen, H. *Sol. Energ. Mat. Sol.* **2013**, *111*, 1.
    DOI: 10.1016/j.solmat.2012.12.016
23. Lussem, B.; Riede, M.; Leo, K.; *Phys. Status Solidi (A)* **2013,** *210*, 9.
    DOI: 10.1002/pssa.201228310
24. Roest, L.; Kelly, J.J.; Vanmaekelbergh, D.; Meulenkamp, E.A. *Phys. Rev. Lett.,* **2002,** *89*, 036801.
    DOI: 10.1103/PhysRevLett.89.036801
25. Kim, J.Y.; Kim, S.H.; Lee, H.H.; Lee, K.; Ma, W.; Gong, X.; Heeger, A.J. *Adv. Mater,* **2006**, *18*, 572.
    DOI: 10.1002/adma.200501825
26. Bundgaard, E.; Krebs, F.C. *Solar Energy Materials and Solar Cells*, **2007**, *91*, 954.
    DOI: 10.1016/j.solmat.2007.01.015
27. Bundgaard, E., Shaheen, S.E., Krebs, F.C., Ginley, D.S. *Solar Energy Materials and Solar Cells*, **2007**, *91*, 1631.
    DOI: 10.1016/j.solmat.2007.05.013
28. Pascui, O.F.; Lohwasser, R.; Sommer, M.; Thelakkat, M.; Thurn-Albrecht, T.; Saalwächter, K. *Macromolecules*, **2010**, *43*, 9401.
    DOI: 10.1021/ma102205t
29. Sun, Y.; Cui, C.; Wang, H.; Li, Y. *Advanced Energy Materials*, **2011**, *1*, 1058.
    DOI: 10.1002/aenm.201100378